A Special Kind of Sliding Mode Control for Nonlinear System With State Constraints

ZHI CHEN[1], **XIAOWEI TU**[1], **LI XING**[1], **JIAN FU**[2], **AND ROGELIO LOZANO**[3]

[1]School of Mechatronic Engineering and Automation, Shanghai University, Shanghai 200072, China
[2]College of Energy and Power Engineering, Nanjing University of Science and Technology, Nanjing 210094, China
[3]UTC-CNRS UMR 7253 Heudiasyc, 60200 Compiegne, France

Corresponding authors: Zhi Chen (andychen183@shu.edu.cn) and Jian Fu (fujian@njust.edu.cn)

ABSTRACT This paper presents a control strategy named auxiliary surfaces sliding mode control (AS-SMC) by using Positive Invariant Set (PIS) to control a class of continuous nonlinear systems with state constraints. The PIS can be regarded as a special kind of sliding surface, and its invariance ensures that the system state can satisfy the constraints in the convergence process. The stability analysis and a PIS theory proof are given. The control strategy is successfully tested in numerical simulations and even effectively applied to the coaxial unmanned helicopter flight control system on hardware in the loop (HIL) platform. The results verify the effectiveness of the proposed control strategy for the experimental set-up.

INDEX TERMS Nonlinear system, positive invariant set (PIS), auxiliary surfaces (AS), sliding mode control (SMC), state constraints.

I. INTRODUCTION

Sliding Mode Control (SMC) is widely used in practical applications for its robust to bounded external disturbances and internal dynamics [22], [23], [24], [9], [1], [6], [20], [11], [12], [8]. In order to improve the robustness of satisfying state constraints and to deal with the robustness of actuator constraints, scholars have conducted a series of studies: [10] proposed a nonlinear sliding surface to ensure that the control signal generated by the controller did not exceed the bounds of a system input, but the state constraints were not considered. Reference [18] presented a first attempt of a sliding mode control to consider constraints in the state. Several related methodologies of other researchers also conducted in-depth research on state constraints [15], [16], [19]. Further studies are required to understand how to satisfy the state constraints of the system when using SMC.

Positive Invariant Set(PIS) research has important significance in the study of the state constraints problem in control theory [2], [14], [5], [17], [13], [25], [3], [21]. Among the many studies, there are no discussions on how SMC can be used so that the constraints are satisfied. Reference [7] proposed a Sliding Mode Control With Unidirectional Auxiliary Surfaces (UAS-SMC) by combining the benefit of SMC

and PIS, but the area of the PIS was not large enough to maintain the state within the constraints under some extreme initial conditions. Reference [3] proposed a terminal sliding mode controller with PIS. Although the algorithm improves the computational capability, the real-time performance of the proposed algorithm does not necessarily meets practical engineering requirements.

Many practical engineering problems that have state constraints in the form of physical constraints, saturation, or performance and safety specifications [29], [30]. For example, the attitude of unmanned helicopter should not exceed the safety angle, otherwise it will tip over. However, the external influences, such as the wind, will inevitably produce a significant change in attitude. How to counteract the disturbance to keep the unmanned helicopter safe, this is a typical state constraints problem in flight control.

In this paper, we introduce an Auxiliary Surfaces Sliding Mode Control (AS-SMC) design strategy by using PIS to solve a class of continuous nonlinear system with state constraints. The main contributions of this paper are:

1) The invariance of PIS and the invariance of SMC in sliding mode phase are correlated for the first time to cope with the system state constraints.

2) On the promise of meeting the computational capability, the designed PIS covers the maximum value of the state

---

The associate editor coordinating the review of this manuscript and approving it for publication was Rosario Pecora.

constraints range, so that the control input keeps the system state within the constraints all the time.

3) This paper verifies that the new strategy can be used in engineering application, and it is first applied to the coaxial unmanned helicopter flight control system successfully. The designed PIS can make the unmanned helicopter attitude angle and angular rate (state) not to exceed the maximum constraints, so as to satisfy the flight safety requirements of the unmanned helicopter.

This paper is organized as follows. The second section presents the problem statement. Then AS-UAS by using PIS design steps are described. The stability analysis and PIS theory proof is given in section IV. The experimental results and analysis are given in section V.

II. PROBLEM FORMULATION
Consider the following general nonlinear uncertain system with state constraints:

$$\dot{X} = f(X) + g(X)u + \eta \qquad (1)$$

where $X = [x_1, \cdots, x_j, \cdots, x_n]^T \in \mathbb{R}^n$ is the system state vector and the full-state vector X is available for feedback. $u \in \mathbb{R}^m$ is the control input, $f(X) \in \mathbb{R}^n$, $g(X) \in \mathbb{R}^{n \times m}$ are continuous functions, $\eta = [\eta_1, \cdots, \eta_j, \cdots, \eta_n]^T \in \mathbb{R}^n$ denotes the disturbance. It is assumed that $f(X)$ and $g(X)$ are known, and η is bounded. Throughout this paper, $\mathbb{R}^{n \times m}$ represents the $n \times m$-dimensional Euclidean spaces; $|\cdot|$ denotes the absolute value, $\|\cdot\|$ denotes the euclidean vector norm or the induced matrix 2-norm.

Assumption 1: The disturbance of the system is bounded, that is $|\eta_j| \le v_j$, v_j is a constant, $j \in \{1, \dots, n\}$.

Note 1: For Assumption 1, the uncertainties values do not require accurate upper bound in the actual design process. As long as the approaching law N_i is greater than v_i the requirements of the controller design are satisfied, that is

$$N_i > sup\{-\sum_{j=1}^{n} \omega_{ij_1} \eta_j\}.$$

The state constraints ϖ and the state integral constraints γ are formulated as follows:

$$\varpi = \left\{ \bar{X} \mid \bar{X} = [\bar{x_1}, \cdots, \bar{x_i}, \cdots, \bar{x_m}]^T \in \mathbb{R}^m, n_i \le \bar{x_i} \le m_i \right\}$$

$$\gamma = \{ \int \bar{X} \mid \int \bar{X} = \left[\int \overline{x_1}, \cdots, \int \overline{x_i}, \cdots, \int \overline{x_m} \right]^T \in \mathbb{R}^m,$$

$$p_i \le \int \overline{x_i} \le q_i\} \qquad (2)$$

where $\bar{x_i} = \sum_{j=1}^{n} I_{ij}x_j$, $\int \bar{x_i} = \sum_{j=1}^{n} \xi_{ij} \int x_j$, I_{ij}, ξ_{ij} and n_j, m_j, p_j, q_j are constant values, $i \in \{1, \cdots, m\}, j \in \{1, \cdots, n\}$. The state constraints and the state integral constraints can also be expressed in the graphical form shown in Figure 1. The yellow shaded area between $\bar{x_i} \in [n_i, m_i]$ and $\int \bar{x_i} \in [p_i, q_i]$ shows the constraints region. Lines S_{1i}, S_{2i}, S_{3i} are the switching surfaces. Quadrangular $P_{S1i+}P_{S1i-}P_{S2i+}P_{S2i-}$ shown in

blue color is the PIS proposed by [7]. Point P indicates the system state initial value. Points P_N and P_U indicate the minimum value of system state following the normal SMC method and the UAS-SMC method respectively. The system state may exceed the state constraints following the normal SMC method, while the UAS-SMC takes advantage of the PIS to constraint the system state, the situation is improved to a certain degree. However, if the system state initial value is outside the PIS, then we cannot guarantee that the state is always in the range of the constraints. In that case it is necessary to extend the PIS as much as possible. The controller should be such that the system state evolves along the ideal red line shown in Figure 1.
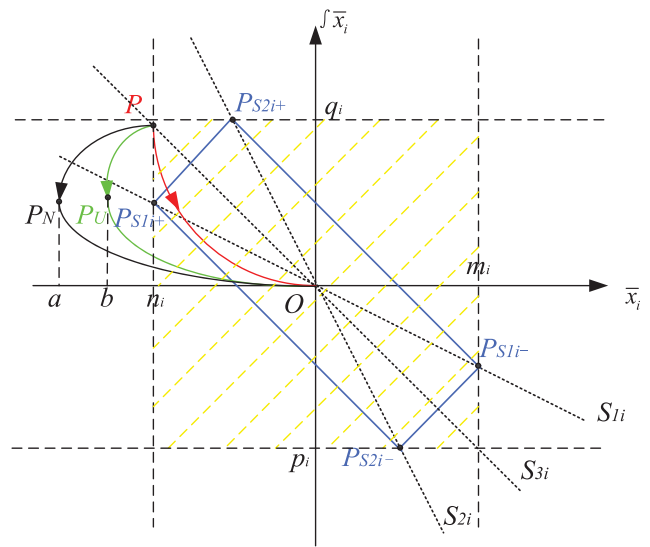

FIGURE 1. The trajectory of system state and its constraints.

The proposed strategy preserves the robustness, while at the same time contains and expands the positive invariant set formed by four auxiliary surfaces in the original proposal to an enlarged positive invariant set formed by six auxiliary surfaces, leading to superiority in control effects within nonlinear system. Linking the state constraints to the PIS makes good use of the excellent properties of the positive invariant set: the system state entering the PIS always runs within it until it tends to the origin. Whether the considered state can satisfy the constraints becomes the problem that the considered state is inside the positive invariant set. If the system state is inside the positive invariant set, the state constraints can be satisfied.

III. AUXILIARY SURFACES SLIDING MODE CONTROLLER DESIGN
Before we design the AS-SMC using PIS formed by six auxiliary surfaces, the traditional integral sliding mode control method is first introduced. The form of its sliding surface is often designed as

$$S(X) = C[X, \int X]^T = 0 \qquad (3)$$

and the approaching law N of the integral sliding mode control can be designed as:

$$N = \dot{S}(X) = -\varepsilon \tanh(S), \quad \varepsilon > 0 \tag{4}$$

where $X = [x_1, \cdots, x_j, \cdots, x_n]^T \in R^n$, $\int X = [\int x_1, \cdots, \int x_j, \cdots, \int x_n]^T$, the term $\int x_j \, dt$ is denoted as $\int x_j$, $S(X) = [S_1(X), \cdots, S_i(X), \cdots, S_m(X)]^T \in R^m$, $C = [I, D] \in R^{m \times 2n}$, $I = [I_1, \cdots, I_i, \cdots, I_m]^T \in R^{m \times n}$, $D = [C_1, \cdots, C_i, \cdots, C_m]^T \in R^{m \times n}$, $C_i = [\xi_{i1}, \cdots, \xi_{in}] \in R^{1 \times n}$, $I_i = [I_{i1}, \cdots, I_{in}] \in R^{1 \times n}$. The hyperbolic tangent function tanh(*) is used to substitute the symbolic function sgn(*). For the i-th switching surface $S_i(X)$ in (3), its representation can be written as:

$$S_i(X) = \sum_{j=1}^{n} (I_{ij} x_j + \xi_{ij} \int x_j), \quad i \in \{1, \cdots, m\} \tag{5}$$

Similar to the traditional integral sliding mode control, the AS-SMC for (1) can be designed using the following steps:

Step1: Select the appropriate switching surfaces $S_{1i}(X)$, $S_{2i}(X)$, and $S_{3i}(X)$

$$\begin{cases} S_{1i}(X) = \sum_{j=1}^{n} (I_{1ij} x_j + \xi_{1ij} \int x_j); \\ S_{2i}(X) = \sum_{j=1}^{n} (I_{2ij} x_j + \xi_{2ij} \int x_j); \\ S_{3i}(X) = \sum_{j=1}^{n} (I_{3ij} x_j + \xi_{3ij} \int x_j); \end{cases} \tag{6}$$

where $S_{1i}(X), S_{2i}(X), S_{3i}(X)$ exists, $\bar{x}_i = \sum_{j=1}^{n} I_{ij} x_j$, $\int \bar{x}_i = \sum_{j=1}^{n} \xi_{ij} \int x_j$, $I_{1ij}, I_{2ij}, I_{3ij}, \xi_{1ij}, \xi_{2ij}, \xi_{3ij}$ are the switching surface gains, $\sum_{j=1}^{n} \xi_{1ij} > 0, \sum_{j=1}^{n} \xi_{2ij} > 0, \sum_{j=1}^{n} \xi_{3ij} > 0$, and $I_{1ij} = I_{2ij} = I_{3ij} = I_{ij}, \xi_{1ij} = \tau_1 \cdot \xi_{ij}, \xi_{2ij} = \tau_2 \cdot \xi_{ij}, \xi_{3ij} = \tau_3 \cdot \xi_{ij}, \tau_1 > \tau_3 > \tau_2$.

Step2: The two-dimensional space $(\bar{x}_i, \int \bar{x}_i)$ expanded by $\bar{x}_i$ and $\int \bar{x}_i$ are divided into six subspaces by switching surfaces S_{1i}, S_{2i}, S_{3i}. The *No.0$_i$*, 1$_i$, 2$_i$, 3$_i$, 4$_i$, 5$_i$ subspaces can be defined as in Figure 2, where

$$No.0_i = \left\{ (\bar{x}_i, \int \bar{x}_i) \mid S_{1i} < 0, S_{2i} < 0, S_{3i} < 0 \right\}$$

$$No.1_i = \left\{ (\bar{x}_i, \int \bar{x}_i) \mid S_{1i} < 0, S_{2i} \geqslant 0, S_{3i} < 0 \right\}$$

$$No.2_i = \left\{ (\bar{x}_i, \int \bar{x}_i) \mid S_{1i} < 0, S_{2i} \geqslant 0, S_{3i} \geqslant 0 \right\}$$

$$No.3_i = \left\{ (\bar{x}_i, \int \bar{x}_i) \mid S_{1i} \geqslant 0, S_{2i} \geqslant 0, S_{3i} \geqslant 0 \right\}$$

$$No.4_i = \left\{ (\bar{x}_i, \int \bar{x}_i) \mid S_{1i} \geqslant 0, S_{2i} < 0, S_{3i} \geqslant 0 \right\}$$

$$No.5_i = \left\{ (\bar{x}_i, \int \bar{x}_i) \mid S_{1i} \geqslant 0, S_{2i} < 0, S_{3i} < 0 \right\} \tag{7}$$
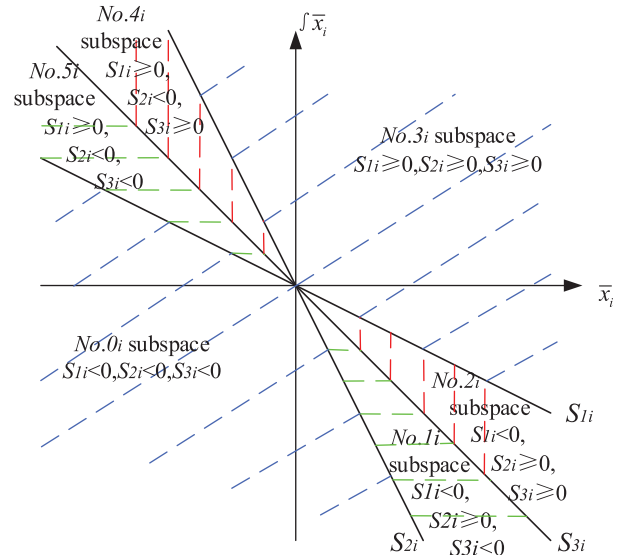

FIGURE 2. The switching surfaces S_{1i}, S_{2i}, S_{3i} divide the state space into six subspaces.
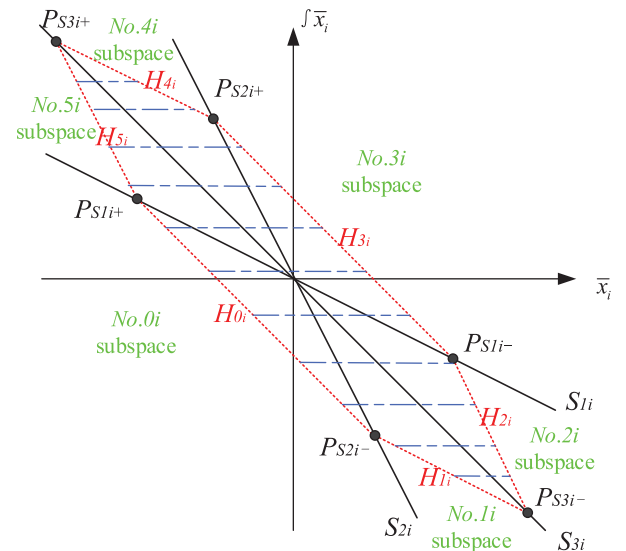

FIGURE 3. *No.0$_i$*, $\cdots$, 5$_i$ subspaces and the auxiliary surfaces $H_{0i}, \cdots, H_{5i}$.

Then, according to the state constraints, points P_{S1i+}, $P_{S1i-}, P_{S2i+}, P_{S2i-}, P_{S1i+}, P_{S1i-}$ (presented in Figure 3) are selected to fulfill the following conditions:

$$S_{1i}(P_{S1i+}) = 0, S_{1i}(P_{S1i-}) = 0$$
$$S_{2i}(P_{S2i+}) = 0, S_{2i}(P_{S2i-}) = 0$$
$$S_{3i}(P_{S3i+}) = 0, S_{3i}(P_{S3i-}) = 0 \tag{8}$$

Points $P_{S1i+}, P_{S1i-}, P_{S2i+}, P_{S2i-}, P_{S3i+}, P_{S3i-}$ are connected to constitute a convex hexagon $\triangle$. The lines $P_{S1i+}P_{S2i-}, P_{S2i-}P_{S3i-}, P_{S3i-}P_{S1i-}, P_{S1i-}P_{S2i+}, P_{S2i+}P_{S3i+}, P_{S3i+}P_{S1i+}$ are auxiliary surfaces $H_{0i}, H_{1i}, H_{2i}, H_{3i}, H_{4i}, H_{5i}$ respectively. The equations of these auxiliary surfaces are expressed as:

$$H_{ki} = \sum_{j=1}^{n} (\omega_{kij_1} x_j + \omega_{kij_2} \int x_j + M_{kij}) \tag{9}$$

where $\omega_{kij_1} \neq 0$, $M_{kij} > 0$, and the subscript $k \in \{0, \cdots, 5\}$ in H_{ki}, ω_{kij_1}, ω_{kij_2} denotes the serial number of the subspaces, the subscript j_1 in ω_{kij_1} denotes the first coefficient and j_2 in ω_{kij_2} denotes the second coefficient, and the subscript $i \in \{1, \cdots, m\}$ indicates the i-th switching surface of $S(X)$. Auxiliary surfaces $H_{0i} = 0$, $H_{1i} = 0$, $H_{2i} = 0$, $H_{3i} = 0$, $H_{4i} = 0$, $H_{5i} = 0$ represent lines $P_{S1i+}P_{S2i-}$, $P_{S2i-}P_{S3i-}$, $P_{S3i-}P_{S1i-}$, $P_{S1i-}P_{S2i+}$, $P_{S2i+}P_{S3i+}$, $P_{S3i+}P_{S1i+}$ in their 2D space. The set $Q = \left\{ (\bar{x}_i, \int \bar{x}_i) \mid H_{ki} \geqslant 0, k = 0, 1, \cdots, 5. \right\}$ denotes all points inside convex hexagon $\triangle$. Q is a positive invariant set as will be demonstrated in section IV.

Step3: Similar to the normal integral sliding mode switching surface $S_i(X)$ shown in (5), the current AS-SMC switching surface $H_i(X)$ can be expressed as:

$$H_i(X) = \sum_{j=1}^{n} \left(\omega_{ij_1} x_j + \omega_{ij_2} \int x_j + m_{ij} \right) \quad (10)$$

where

$$\omega_{ij_1} = \begin{cases} \omega_{0ij_1}, & No.0_i \\ \omega_{1ij_1}, & No.1_i \\ \omega_{2ij_1}, & No.2_i \\ \omega_{3ij_1}, & No.3_i \\ \omega_{4ij_1}, & No.4_i \\ \omega_{5ij_1}, & No.5_i \end{cases} \quad \omega_{ij_2} = \begin{cases} \omega_{0ij_2}, & No.0_i \\ \omega_{1ij_2}, & No.1_i \\ \omega_{2ij_2}, & No.2_i \\ \omega_{3ij_2}, & No.3_i \\ \omega_{4ij_2}, & No.4_i \\ \omega_{5ij_2}, & No.5_i \end{cases}$$

$$m_{ij} = \begin{cases} M_{0ij}, & No.0_i \\ M_{1ij}, & No.1_i \\ M_{2ij}, & No.2_i \\ M_{3ij}, & No.3_i \\ M_{4ij}, & No.4_i \\ M_{5ij}, & No.5_i \end{cases}$$

For the special sliding surface $H_i(X)$ of the AS-SMC, the coefficients ω_{ij_1} and ω_{ij_2} can be calculated according to the state constraints ϖ, the state integral constraints γ, and the switching surface gains $\xi_{1ij}, \xi_{2ij}, \xi_{3ij}$. The calculation steps are as follows:

i) Determine the point P_{s3i+} and point P_{s3i-}

According to the state constraints ϖ and the state integral constraints γ, the point $P_{s3i+}(-\xi_{3ij}, 1)$ and the point $P_{s3i-}(\xi_{3ij}, -1)$ are chosen on switching surface S_{3i} in order to satisfy the state constraints and the integral constraints simultaneously.

ii) Determine the points P_{s1i+}, P_{s1i-} and the points P_{s2i+}, P_{s2i-}

According to the parallel property (20), the slope of switching surface $S_{2i} = 0$ and the point coordinates $P_{s3i+}(-\xi_{3ij}, 1)$ and $P_{s3i-}(\xi_{3ij}, -1)$, the lines $P_{s3i+}P_{s1i+}$ and $P_{s3i-}P_{s1i-}$ are obtained by the point oblique equation. Where the auxiliary surface $H_{5i}(P_{s3i+}P_{s1i+})$ is $\int x_i - 1 = \xi_{2ij}(x_i + \xi_{3ij})$, the auxiliary surface $H_{2i}(P_{s3i-}P_{s1i-})$ is $\int x_i + 1 = \xi_{2ij}(x_i - \xi_{3ij})$. The two auxiliary surfaces intersect the switching surface $S_{1i} = 0$ at P_{s1i+} and P_{s1i-}, respectively. The point coordinates of P_{s1i+} and P_{s1i-} are $P_{s1i+} \left(-\frac{\xi_{1ij}(1+\xi_{2ij}\xi_{3ij})}{1+\xi_{1ij}\xi_{2ij}}, \frac{1+\xi_{2ij}\xi_{3ij}}{1+\xi_{1ij}\xi_{2ij}} \right)$ and

$P_{s1i-} \left(\frac{\xi_{1ij}(1+\xi_{2ij}\xi_{3ij})}{1+\xi_{1ij}\xi_{2ij}}, -\frac{1+\xi_{2ij}\xi_{3ij}}{1+\xi_{1ij}\xi_{2ij}} \right)$. Similarly, according to the parallel property (20), the slope of switching surface $S_{1i} = 0$ and the point coordinates $P_{s3i+}(-\xi_{3ij}, 1)$ and $P_{s3i-}(\xi_{3ij}, -1)$, the auxiliary surfaces $H_{4i}(P_{s3i+}P_{s2i+})$ and $H_{1i}(P_{s3i-}P_{s2i-})$ are obtained by the point oblique equation. Where the auxiliary surface $H_{4i}(P_{s3i+}P_{s2i+})$ is $\int x_i - 1 = \xi_{1ij}(x_i + \xi_{3ij})$, the auxiliary surface $H_{1i}(P_{s3i-}P_{s2i-})$ is $\int x_i + 1 = \xi_{1ij}(x_i - \xi_{3ij})$. The two auxiliary surfaces intersect the switching surface $S_{2i} = 0$ at $P_{s2i+} \left(-\frac{\xi_{2ij}(1+\xi_{1ij}\xi_{3ij})}{1+\xi_{1ij}\xi_{2ij}}, \frac{1+\xi_{1ij}\xi_{3ij}}{1+\xi_{1ij}\xi_{2ij}} \right)$ and $P_{s2i-} \left(\frac{\xi_{2ij}(1+\xi_{1ij}\xi_{3ij})}{1+\xi_{1ij}\xi_{2ij}}, -\frac{1+\xi_{1ij}\xi_{3ij}}{1+\xi_{1ij}\xi_{2ij}} \right)$, respectively. It is easy to get the following results: $\omega_{1ij_1} = \xi_{1ij}$, $\omega_{1ij_2} = 1$, $M_{1ij} = -1 - \xi_{2ij}\xi_{3ij}$, $\omega_{2ij_1} = \xi_{2ij}$, $\omega_{2ij_2} = 1$, $M_{2ij} = -1 - \xi_{2ij}\xi_{3ij}$, $\omega_{4ij_1} = \xi_{1ij}$, $\omega_{4ij_2} = 1$, $M_{4ij} = 1 + \xi_{1ij}\xi_{3ij}$, $\omega_{5ij_1} = \xi_{2ij}$, $\omega_{5ij_2} = 1$, $M_{5ij} = 1 + \xi_{2ij}\xi_{3ij}$.

iii) Determine the ω_{0ij_1}, ω_{0ij_2}, M_{0ij}, ω_{3ij_1}, ω_{3ij_2}, M_{3ij}

Since the coordinates of points P_{s1i+}, P_{s1i-}, P_{s2i+}, and P_{s2i-} are obtained by i) and ii), and according to the two-point coordinate equation, the auxiliary surfaces $H_{0i}(P_{s1i+}P_{s2i-})$ and $H_{3i}(P_{s2i+}P_{s1i-})$ are obtained. Where the auxiliary surface H_{0i} is $(\int x_i + \frac{1+\xi_{1ij}\xi_{3ij}}{1+\xi_{1ij}\xi_{2ij}})/(\frac{1+\xi_{2ij}\xi_{3ij}}{1+\xi_{1ij}\xi_{2ij}} + \frac{1+\xi_{1ij}\xi_{3ij}}{1+\xi_{1ij}\xi_{2ij}}) = (x_i - \frac{\xi_{2ij}(1+\xi_{1ij}\xi_{3ij})}{1+\xi_{1ij}\xi_{2ij}})/(-\frac{\xi_{1ij}(1+\xi_{2ij}\xi_{3ij})}{1+\xi_{1ij}\xi_{2ij}} - \frac{\xi_{2ij}(1+\xi_{1ij}\xi_{3ij})}{1+\xi_{1ij}\xi_{2ij}})$, the auxiliary surface H_{3i} is $(\int x_i + \frac{1+\xi_{2ij}\xi_{3ij}}{1+\xi_{1ij}\xi_{2ij}})/(\frac{1+\xi_{1ij}\xi_{3ij}}{1+\xi_{1ij}\xi_{2ij}} + \frac{1+\xi_{2ij}\xi_{3ij}}{1+\xi_{1ij}\xi_{2ij}}) = (x_i - \frac{\xi_{1ij}(1+\xi_{2ij}\xi_{3ij})}{1+\xi_{1ij}\xi_{2ij}})/(-\frac{\xi_{1ij}(1+\xi_{2ij}\xi_{3ij})}{1+\xi_{1ij}\xi_{2ij}} - \frac{\xi_{1ij}(1+\xi_{2ij}\xi_{3ij})}{1+\xi_{1ij}\xi_{2ij}})$. Thus we got $\omega_{0ij_1} = 1/(-\frac{\xi_{1ij}(1+\xi_{2ij}\xi_{3ij})}{1+\xi_{1ij}\xi_{2ij}} - \frac{\xi_{2ij}(1+\xi_{1ij}\xi_{3ij})}{1+\xi_{1ij}\xi_{2ij}})$, $\omega_{0ij_2} = 1/(\frac{1+\xi_{2ij}\xi_{3ij}}{1+\xi_{1ij}\xi_{2ij}} + \frac{1+\xi_{1ij}\xi_{3ij}}{1+\xi_{1ij}\xi_{2ij}})$, $M_{0ij} = \frac{\xi_{2ij}(1+\xi_{1ij}\xi_{3ij})}{1+\xi_{1ij}\xi_{2ij}}/(-\frac{\xi_{1ij}(1+\xi_{2ij}\xi_{3ij})}{1+\xi_{1ij}\xi_{2ij}} + \frac{\xi_{2ij}(1+\xi_{1ij}\xi_{3ij})}{1+\xi_{1ij}\xi_{2ij}}) - \frac{1+\xi_{1ij}\xi_{3ij}}{1+\xi_{1ij}\xi_{2ij}}/(\frac{1+\xi_{2ij}\xi_{3ij}}{1+\xi_{1ij}\xi_{2ij}} + \frac{1+\xi_{1ij}\xi_{3ij}}{1+\xi_{1ij}\xi_{2ij}})$, $\omega_{3ij_1} = 1/(\frac{\xi_{1ij}(1+\xi_{2ij}\xi_{3ij})}{1+\xi_{1ij}\xi_{2ij}} - \frac{\xi_{1ij}(1+\xi_{2ij}\xi_{3ij})}{1+\xi_{1ij}\xi_{2ij}})$, $\omega_{3ij_2} = 1/(\frac{1+\xi_{1ij}\xi_{3ij}}{1+\xi_{1ij}\xi_{2ij}} + \frac{1+\xi_{2ij}\xi_{3ij}}{1+\xi_{1ij}\xi_{2ij}})$, and finally $M_{3ij} = -\frac{1+\xi_{2ij}\xi_{3ij}}{1+\xi_{1ij}\xi_{2ij}}/(\frac{1+\xi_{1ij}\xi_{3ij}}{1+\xi_{1ij}\xi_{2ij}} + \frac{1+\xi_{2ij}\xi_{3ij}}{1+\xi_{1ij}\xi_{2ij}}) - \frac{\xi_{1ij}(1+\xi_{2ij}\xi_{3ij})}{1+\xi_{1ij}\xi_{2ij}}/(\frac{\xi_{1ij}(1+\xi_{2ij}\xi_{3ij})}{1+\xi_{1ij}\xi_{2ij}} - \frac{\xi_{1ij}(1+\xi_{2ij}\xi_{3ij})}{1+\xi_{1ij}\xi_{2ij}})$.

Step4: Referring to the form of (5), we rewrite (10) as follow:

$$H_i(X) = \sum_{j=1}^{n} \left(w_{ij_1} x_j + w_{ij_2} \int x_j \right) + \sum_{j=1}^{n} m_{ij}, i \in \{1, \cdots, m\} \quad (11)$$

That is

$$H_i(X) = \hat{C}_i [x_j, \int x_j]^T + M_i \quad (12)$$

where $\hat{C}_i = [\hat{C}_{i1}, \hat{C}_{i2}]$, $\hat{C}_{i1} = [\omega_{i1_1}, \cdots, \omega_{in_1}] \in R^{1 \times n}$, $\hat{C}_{i2} = [\omega_{i1_2}, \cdots, \omega_{in_2}] \in R^{1 \times n}$, $M_i = \sum_{j=1}^{n} m_{ij}$, $i \in \{1, \cdots, m\}$

Referring to the form of (3), the AS sliding surface can be written in a compact form:

$$H = \hat{C}[X, \int X]^T + M \quad (13)$$

where $H = [H_1, \cdots, H_i, \cdots, H_m]^T \in R^m$, $\hat{C} = [\Omega_1, \Omega_2] \in R^{m \times 2n}$, $\Omega_1 = [\hat{C}_{11}, \cdots, \hat{C}_{i1}, \cdots, \hat{C}_{m1}]^T \in R^{m \times n}$, $\Omega_2 = [\hat{C}_{12}, \cdots, \hat{C}_{i2}, \cdots, \hat{C}_{m2}]^T \in R^{m \times n}$, $M = [M_1, \cdots, M_m]^T \in R^m$.

By solving the differential equation $\dot{H}(u) = N$, we can design the AS sliding mode control law for (1) of the form

$$u = [\Omega_1 g(X)]^{-1}[-\Omega_1 f(X) - \Omega_2 X + N] \quad (14)$$

where the approaching law $N = diag[N_1, \cdots, N_i, \cdots, N_m]^T$, and $N_i > sup\{-\sum_{j=1}^{n} \omega_{ij_1}\eta_j\}$.
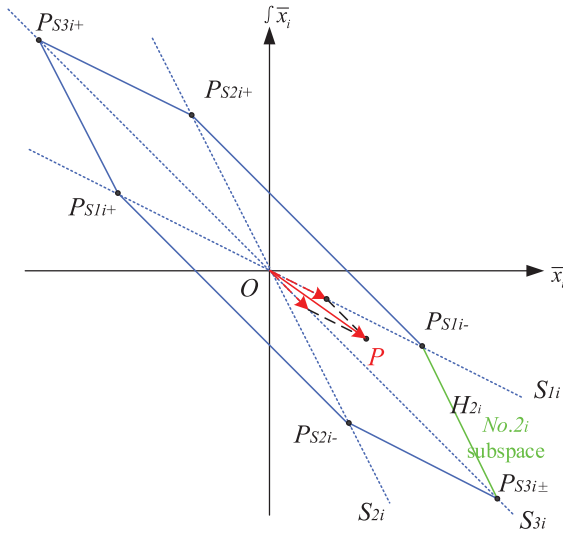

FIGURE 4. Point P coordinate transformation schematic diagram.

IV. THE AUXILIARY SURFACES SLIDING MODE CONTROL STABILITY PROOF

Lemma 1: Point $P_j(x_j, y_j) = P_j(x_j, \int x_j)$ is located in $No.k_i$ subspace for the state x_j as shown in Figure 4. Any two adjacent points in points $P_{S1i\pm}, P_{S2i\pm}, P_{S3i\pm} \in \{P_{S1i+}, P_{S1i-}, P_{S2i+}P_{S2i-}, P_{S3i+}, P_{S3i-}\}$ constitute the local auxiliary surface (15) in $No.k_i$ subspace.

$$H_{ki}(P_j) = \omega_{kij_1}x_j + \omega_{kij_2}\int x_j + M_{kij}, \quad M_{kij} > 0 \quad (15)$$

Thus for the point P_j, we have $M_{kij} - H_{ki}(P_j) \geqslant 0$, and $P_j(0,0)$ if and only if $H_{ki}(P_j) = M_{kij}$.

Proof: Reference to Appendix A in [26]. □

Lemma 2: For the point set $P(t) = \{P_1(x_1(t), y_1(t)), \cdots, P_j(x_j(t), y_j(t)), \cdots, P_n(x_n(t), y_n(t))\}$, which is on the auxiliary surface (9), we have

$$H_{ki}(P) = \sum_{j=1}^{n} H_{ki}(P_j) = \sum_{j=1}^{n}(\omega_{kij_1}x_j + \omega_{kij_2}\int x_j + M_{kij}) \quad (16)$$

where $M_{kij} > 0$. Thus for the point set P, we have $\sum_{j=1}^{n} M_{kij} - H_{ki}(P) \geqslant 0$, and $P = \{P_1(0,0), \cdots, P_j(0,0), \cdots, P_n(0,0)\}$ if and only if $H_{ki}(P) = \sum_{j=1}^{n} M_{kij}$.

Proof: Without loss of generality, points $P_{S1i-} = (x_j^1, y_j^1)$ and $P_{S3i-} = (x_j^3, y_j^3)$ are connected to form the

auxiliary surface H_{2i}. Since points P_{S1i-} and P_{S3i-} are on the line of the auxiliary surface H_{2i}, we have

$$\begin{cases} H_{2i}(P_{S1i\pm}) = \sum_{j=1}^{n}(\omega_{2ij_1}x_j^1 + \omega_{2ij_2}y_j^1 + M_{2ij}) = 0 \\ H_{2i}(P_{S3i\pm}) = \sum_{j=1}^{n}(\omega_{2ij_1}x_j^3 + \omega_{2ij_2}y_j^3 + M_{2ij}) = 0 \end{cases} \quad (17)$$

Since point P_j is located in the $No.2_i$ subspace, we have

$$\overrightarrow{OP_j} = k_j^1 \overrightarrow{OP_{jS1i\pm}} + k_j^2 \overrightarrow{OP_{jS3i\pm}}, \quad k_j^1 \geqslant 0, \ k_j^2 \geqslant 0$$

Thus, the coordinates of point P_j can be converted into the following expression

$$P_j = ((k_j^1 x_j^1 + k_j^2 x_j^3), (k_j^1 y_j^1 + k_j^2 y_j^3)) \quad (18)$$

Substituting (18) into (16), we have

$$\begin{aligned} &H_{2i}(P) \\ &= \sum_{j=1}^{n}[\omega_{2ij_1}(k_j^1 x_j^1 + k_j^2 x_j^3) + \omega_{2ij_2}(k_j^1 y_j^1 + k_j^2 y_j^3) + M_{2ij}] \\ &= \sum_{j=1}^{n}[k_j^1(\omega_{2ij_1}x_j^1 + \omega_{2ij_2}y_j^1) + k_j^2(\omega_{2ij_1}x_j^3 + \omega_{2ij_2}y_j^3) + M_{2ij}] \\ &= \sum_{j=1}^{n}[k_j^1(\omega_{2ij_1}x_j^1 + \omega_{2ij_2}y_j^1 + M_{2ij}) \\ &\quad + k_j^2(\omega_{2ij_1}x_j^3 + \omega_{2ij_2}y_j^3 + M_{2ij}) - (k_j^1 M_{2ij} + k_j^2 M_{2ij}) + M_{2ij}] \end{aligned} \quad (19)$$

Substituting (17) into (19), we have

$$H_{2i}(P) = \sum_{j=1}^{n}[-(k_j^1 M_{2ij} + k_j^2 M_{2ij}) + M_{2ij}]$$

Thus

$$\sum_{j=1}^{n} M_{2ij} - H_{2i}(P) = \sum_{j=1}^{n}[(k_j^1 M_{2ij} + k_j^2 M_{2ij})]$$

Since $k_j^1 \geqslant 0, k_j^2 \geqslant 0, M_{2ij} > 0$, we thus have

$$\sum_{j=1}^{n} M_{2ij} - H_{2i}(P) \geqslant 0$$

Without loss of generality, any auxiliary surface which is located in $No.k_i$ subspace has the following conclusion:

$$\sum_{j=1}^{n} M_{kij} - H_{ki}(P) \geqslant 0$$

When $H_{ki}(P) = \sum_{j=1}^{n} M_{kij}$, since $k_j^1 \geqslant 0, k_j^2 \geqslant 0, M_{kij} > 0$, we get $k_j^1 = 0, k_j^2 = 0$. And from (18), we have $P = \{P_1(0,0), \cdots, P_j(0,0), \cdots, P_n(0,0)\}$ if and only if $H_{ki}(P) = \sum_{j=1}^{n} M_{kij}$. □
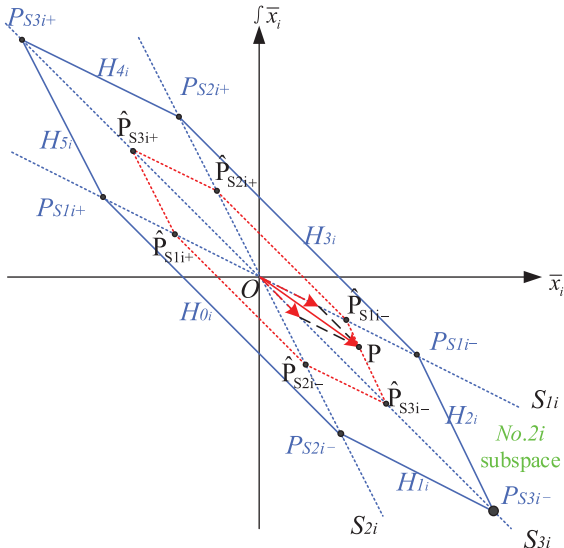
FIGURE 5. The movement of point P_j in *No.k_i* subspace schematic diagram.

Definition 3: Points $\hat{P}_{S2i+}\hat{P}_{S3i+}\hat{P}_{S1i+}\hat{P}_{S2i-}\hat{P}_{S3i-}\hat{P}_{S1i-}$ *are connected to form a convex hexagon δ, Points* $P_{S2i+}P_{S3i+}P_{S1i+}P_{S2i-}P_{S3i-}P_{S1i-}$ *are connected to form a convex hexagon Δ. As shown in Figure 5, the sides of the convex hexagon δ and Δ have the following properties:*

$$
\begin{cases}
\hat{P}_{S2i+}\hat{P}_{S3i+} \parallel P_{S2i+}P_{S3i+} \parallel \hat{P}_{S1i+}\hat{P}_{S1i-} \\
\parallel \hat{P}_{S2i-}\hat{P}_{S3i-} \parallel P_{S2i-}P_{S3i-} \\
\hat{P}_{S3i+}\hat{P}_{S1i+} \parallel P_{S3i+}P_{S1i+} \parallel \hat{P}_{S2i+}\hat{P}_{S2i-} \\
\parallel \hat{P}_{S3i-}\hat{P}_{S1i-} \parallel P_{S3i-}P_{S1i-} \\
\hat{P}_{S1i+}\hat{P}_{S2i-} \parallel P_{S1i+}P_{S2i-} \parallel \hat{P}_{S3i+}\hat{P}_{S3i-} \\
\parallel \hat{P}_{S1i-}\hat{P}_{S2i+} \parallel P_{S1i-}P_{S2i+}
\end{cases}
\tag{20}
$$

where the symbol $\parallel$ indicates parallel. Point set $P(t)$ is on the boundary of the convex hexagon δ.

1) If $H_{ki}(P(t)) \geqslant 0, k = 0, \cdots, 5$, then point set $P(t)$ is inside the convex hexagon Δ.

2) If $H_{ki}(P(t)) < 0, k = 0, \cdots, 5$, then point set $P(t)$ is outside the convex hexagon Δ.

Theorem 4: For nonlinear system (1), the controller (14) can guarantee the closed loop system state $X = [x_1, \cdots, x_j, \cdots, x_n]^T$ asymptotically stable and the convex set

$$
Q = \left\{ (\bar{x}_i, \int \bar{x}_i) \mid H_{ki}(P(t)) \geqslant 0 \right\}, \quad i \in \{1, \cdots, m\},
$$
$$
k = 0, \cdots, 5. \tag{21}
$$

is a positive invariant set. In other words, for point set $P(t) = \{P_1(x_1(t), y_1(t)), \cdots, P_j(x_j(t), y_j(t)), \cdots, P_n(x_n(t), y_n(t))\}$, if there is $P(t_0)$ inside the convex hexagon Δ, then for $t > t_0$, $P(t)$ is also inside the convex hexagon Δ.

Proof: 1) First the stability proof is given.

For the point set $P = \{P_1(x_1, y_1), \cdots, P_j(x_j, y_j), \cdots, P_n(x_n, y_n)\}$, we construct the convex hexagons Δ according to

Definition 1. A candidate Lyapunov function is chosen as

$$
V = \frac{1}{2} \left[\frac{\sum\limits_{j=1}^{n} M_{kij} - H_{ki}(P(t))}{\sum\limits_{j=1}^{n} M_{kij}} \right]^2
\tag{22}
$$

First of all, $V \geqslant 0$ will be proved, and if $V = 0$, then $X = 0$.

From (22), it is easy to know that $V \geqslant 0$. When $V = 0$, we have $H_{ki}(P(t)) = \sum\limits_{j=1}^{n} M_{kij}$. And according to Lemma IV.2, $H_{ki}(P(t)) = \sum\limits_{j=1}^{n} M_{kij}$ means $P = \{P_1(0, 0), \cdots, P_j(0, 0), \cdots, P_n(0, 0)\}$. Thus we have $V \geqslant 0$, and if $V = 0$, $X = [x_1, \cdots, x_n]^T = 0$

Then, $\dot{V} < 0$ will be proved if $X \neq 0$. Differentiating (22), we obtain

$$
\dot{V} = -\frac{\sum\limits_{j=1}^{n} M_{kij} - H_{ki}(P(t))}{\sum\limits_{j=1}^{n} M_{kij}} \cdot \dot{H}_{ki}(P(t))
\tag{23}
$$

From Lemma IV.2, we have $\sum\limits_{j=1}^{n} M_{kij} - H_{ki}(P(t)) \geqslant 0$. And when $\sum\limits_{j=1}^{n} M_{kij} = H_{ki}(P(t))$, we have $X = [x_1, \cdots, x_n]^T = 0$. Thus, $\sum\limits_{j=1}^{n} M_{kij} - H_{ki}(P(t)) > 0$ holds if $X \neq 0$.

Differentiating (13), we obtain

$$
\dot{H} = \Omega_1 \dot{X} + \Omega_2 X + \dot{M}
\tag{24}
$$

Substituting (1) and (14) into $\dot{H}(X)$, we obtain $\dot{H} = N + \Omega_1 \cdot \eta$. Thus the i-th AS switching surface in *No.k_i* subspace is $\dot{H}_{ki} = N_i + \sum\limits_{j=1}^{n} \omega_{ij_1} \eta_j$. And from (14) we know that $N_i > sup\{-\sum\limits_{j=1}^{n} \omega_{ij_1} \eta_j\}$, thus $\dot{H}_{ki}(P(t)) > 0$. Since $\sum\limits_{j=1}^{n} M_{kij} - H_{ki}(P(t)) > 0$, $\dot{H}_{ki}(P(t)) > 0$, $\sum\limits_{j=1}^{n} M_{kij} > 0$, thus according to (23) we have $\dot{V} < 0$.

To sum up, we have the conclusion: if point set $P = \{P_1(x_1, y_1), \cdots, P_n(x_n, y_n)\} \neq \{P_1(0, 0), \cdots, P_n(0, 0)\}$, then $\dot{V} < 0$.

The continuity of Lyapunov function V is also proved. The discussion for the continuity of Lyapunov function V will focus on the point which is switching between adjacent subspaces. Take point $\hat{P}_j(t)$ which is switching between the *No.1$_i$* and *No.2$_i$* subspaces as an example. Without loss of generality, we assume point $\hat{P}_j(t)$ coincides with point $\hat{P}_{S3i-} = \hat{P}_j(x_j, y_j)$ shown as Figure 6. It is apparent that point $\hat{P}_j(t)$ and point $\hat{P}_{S3i-}$ are located on the switching surface $\hat{S}_{3i}$. Then, the coordinate of point $\hat{P}_j(t)$ can be expressed as

$$
\hat{P}_j(t) = \hat{P}_j(\lambda_j x_j, \lambda_j y_j), \quad \lambda_j \geqslant 0
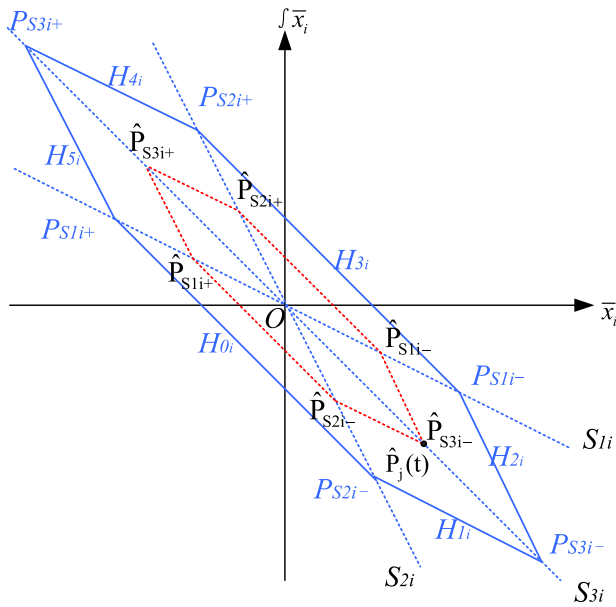\tag{25}
$$

FIGURE 6. *P(t)* is switching between the switching surface S_{3i} and $No.k_i$ subspace.

Invoking (25) into (16), we have

$$
\begin{aligned}
H_{1i}(P) &= \sum_{j=1}^{n} H_{1i}(\hat{P}_j) \\
&= \sum_{j=1}^{n} \lambda_j(\omega_{1ij_1}x_j + \omega_{1ij_2}y_j + M_{1ij}) \\
&\quad + \sum_{j=1}^{n} (-\lambda_j M_{1ij} + M_{1ij}) \\
H_{2i}(P) &= \sum_{j=1}^{n} H_{2i}(\hat{P}_j) \\
&= \sum_{j=1}^{n} \lambda_j(\omega_{1ij_1}x_j + \omega_{2ij_2}y_j + M_{2ij}) \\
&\quad + \sum_{j=1}^{n} (-\lambda_j M_{2ij} + M_{2ij})
\end{aligned}
\tag{26}
$$

Substituting (17) into (26), we have

$$
\begin{aligned}
\sum_{j=1}^{n} H_{1i}(\hat{P}_j) &= \sum_{j=1}^{n} (-\lambda_j M_{1ij} + M_{1ij}) \\
\sum_{j=1}^{n} H_{2i}(\hat{P}_j) &= \sum_{j=1}^{n} (-\lambda_j M_{2ij} + M_{2ij})
\end{aligned}
\tag{27}
$$

Using the normalized method, we can design the auxiliary surface parameters of M_{1ij} equal to M_{2ij}. Since $M_{1ij} = M_{2ij}$, and reference to Lemma IV.2 in (Fu, 2016), we conclude that $H_{1i}(\hat{P}_j) = H_{2i}(\hat{P}_j)$. From (26), we can have a new

conclusion that $H_{1i}(P) = \sum_{j=1}^{n} H_{1i}(\hat{P}_j) = \sum_{j=1}^{n} H_{2i}(\hat{P}_j) = H_{2i}(P)$. Without loss of generality, for the $No.1_i$ and $No.2_i$ subspaces, we have the following equations according to (22):

$$
V_1 = \frac{1}{2}\left[(\sum_{j=1}^{n} M_{1ij} - H_{1i}(P(t)))/M_{1ij} \right]^2
$$

$$
V_2 = \frac{1}{2}\left[(\sum_{j=1}^{n} M_{2ij} - H_{2i}(P(t)))/M_{2ij} \right]^2
\tag{28}
$$

Thus V_1 and V_2 are equal. Therefore, the Lyapunov function V is continuous.

In conclusion, Lyapunov function V is a continuous function. And because $V \geq 0$ (if and only if $X = 0$, then $V = 0$), and $\dot{V} < 0$ (if $X \neq 0$), thus the system state $X = [x_1, \cdots, x_n]^T$ is asymptotically stable.

2) Second, the prove that Q_j is a positive invariant set by using the counter-evidence method:

Consider point $P_j(t_0) = (x_j(t_0), y_j(t_0))$ is inside the convex hexagon Δ. Assuming there exist a point $P_j(t_1) = (x_j(t_1), y_j(t_1))$, $t_1 > t_0$ located outside the convex hexagon Δ. Since $P_j(t_0)$ is inside the convex hexagon Δ, according to Definition 1, we have $H_{ki}(P(t_0)) = \sum_{j=1}^{n} H_{kij}(P_j(t_0)) \geq 0$, thus

$$
V(P(t_0)) = \frac{1}{2}\left[\frac{\sum_{j=1}^{n} M_{kij} - H_{ki}(P(t_0))}{\sum_{j=1}^{n} M_{kij}} \right]^2 \leqslant \frac{1}{2}
$$

Since $P_j(t_1)$ is outside the convex hexagon Δ, from Definition 1 we also have $H_{ki}(P(t_1)) = \sum_{j=1}^{n} H_{kij}(P_j) < 0$, thus $V(P(t_1)) > \frac{1}{2}$.

In conclusion, $V(P(t_0)) \leqslant \frac{1}{2} < V(P(t_1))$ when $t_0 < t_1$. Since V is continuous, thus there must exist $\dot{V}P((t_2) > 0$, where $t_0 < t_2 < t_1$. This conclusion contradicts the above conclusion $\dot{V} < 0$ in the stability proof, thus the assumption is invalid. Therefore, the convex set Q_j is a positive invariant set. The proof is completed. □

V. RESULTS

The auxiliary surfaces sliding mode control by using positive invariant set is tested under different conditions and scenarios.

A. SCENARIO A: AUXILIARY SURFACES SLIDING MODE CONTROL FOR FULL-DRIVE SYSTEM

In numerical simulation, a second-order nonlinear system (29) is chosen as an example to validate the control strategy.

$$
\dot{X} = f(X) + g(X)u + \eta
\tag{29}
$$

where $X = [x_1, x_2]^T$, $\eta = [0.1 sint + 0.1 x_2, 0.1 cost]^T$, $u = [u_1, u_2]^T$

$$f(X) = \begin{bmatrix} x_2 \\ \dfrac{107.9 sinx_1 - 1.5 x_2^2 cosx_1 sinx_1}{7.3 - 1.5 cos(x_1)^2} \end{bmatrix},$$

$$g(X) = \begin{bmatrix} 1 & 0 \\ 0 & (cosx_1)/7.3 - 1.5 cos(x_1)^2 \end{bmatrix}.$$

The state initial values are $x_1(t_0) = 1$, $x_2(t_0) = -1$, $\int_0^{t_0} x_1(\tau) \, d\tau = -1$, $\int_0^{t_0} x_2(\tau) \, d\tau = 1$. The state constraints are

$$\varpi = \left\{ [x_1, x_2]^T \mid -1 \le x_1 \le 1, -1 \le x_2 \le 1 \right\}$$

$$\gamma = \left\{ \left[\int x_1, \int x_2 \right]^T \mid -1 \le \int x_1 \le 1, -1 \le \int x_2 \le 1 \right\}$$

The sliding surface $\acute{S}$ and the approaching law $\acute{N}$ of the normal integral SMC are

$$\acute{S} = \begin{bmatrix} \acute{S}_1 \\ \acute{S}_2 \end{bmatrix} = \begin{bmatrix} I_{11} x_1 + \xi_{11} \cdot \int x_1 \\ I_{22} x_2 + \xi_{22} \cdot \int x_2 \end{bmatrix}, \acute{N} = \begin{bmatrix} -N_1 \cdot tanh(\acute{S}_1) \\ -N_2 \cdot tanh(\acute{S}_2) \end{bmatrix},$$

where $I_{11} = I_{22} = 1$, $\xi_{11} = \xi_{22} = 2$, $N_1 = N_2 = 10$.

The AS-SMC controller design is presented under the steps in Section 3:

First, we select the points $P_{S3i+} = (-1, 1)$ and $P_{S3i-} = (1, -1)$ according to the constraints. Thus, the third sliding surface $S_3(X)$ is constructed as $S_3(X) = X + diag\{1, 1\} \int X$, where $S_3(X) = [S_{31}, S_{32}]^T$. Then, we select the switching surfaces as $S_1(X) = X + diag\{2, 2\} \int X$, $S_2(X) = X + diag\{0.5, 0.5\} \int X$, where $S_1(X) = [S_{11}, S_{12}]^T$, $S_2(X) = [S_{21}, S_{22}]^T$.

Second, for state x_1, according to the parallel property (20), the slope of switching surfaces S_{11} and S_{21} and the point coordinates of $P_{S3i\pm}$, we choose points as $P_{S1i+} = (-0.5, 0, 25)$, $P_{S1i-} = (0.5, -0, 25)$, $P_{S2i+} = (-0, 25, 0.5)$, $P_{S2i-} = (0, 25, -0.5)$.

Third, the current auxiliary surface $H_1 = \omega_{11_1} x_1 + \omega_{11_2} \int x_1 + M_1$ for state x_1 can be obtained, where

$$\omega_{11_1} = \begin{cases} 1, & No.0_i \\ 2, & No.1_i \\ -3, & No.2_i \\ -1, & No.3_i \\ -2, & No.4_i \\ 3, & No.5_i \end{cases} \quad \omega_{11_2} = \begin{cases} 1, & No.0_i \\ 3, & No.1_i \\ -2, & No.2_i \\ -1, & No.3_i \\ -3, & No.4_i \\ 2, & No.5_i \end{cases}$$

$$M_1 = \begin{cases} 0.25, & No.0_i \\ 1, & No.1_i \\ 1, & No.2_i \\ 0.25, & No.3_i \\ 1, & No.4_i \\ 1, & No.5_i \end{cases}$$

The coefficients of state x_2 can be obtained in the same way. In this example, we have $H_2 = \omega_{22_1} x_2 + \omega_{22_2} \int x_2 + M_2$, where $\omega_{11_1} = \omega_{22_1}$, $\omega_{11_2} = \omega_{22_2}$, $M_2 = M_1$.

Finally, the controller $u = [\Omega_1 g(X)]^{-1} [-\Omega_1 f(X) - \Omega_2 X + N]$, where $\Omega_1 = diag\{\omega_{11_2}, \omega_{22_1}\}$, $\Omega_2 = diag\{\omega_{11_2}, \omega_{22_2}\}$, $N = [N_1, N_2]^T = [0.6, 0.3]^T$

The boundary layer SMC (shown as 'Normal' in figures), UAS-SMC using four auxiliary surfaces (shown as 'Quadrangular' in figures) and AS-SMC using six auxiliary surfaces (shown as 'Hexagon' in figures) are compared in Scenario A. All of the controller parameters are given in Table 1. Following the above steps, we get the numerical simulation results shown in Figure 7 through Figure 14 as follows:

TABLE 1. Controller design coefficients.

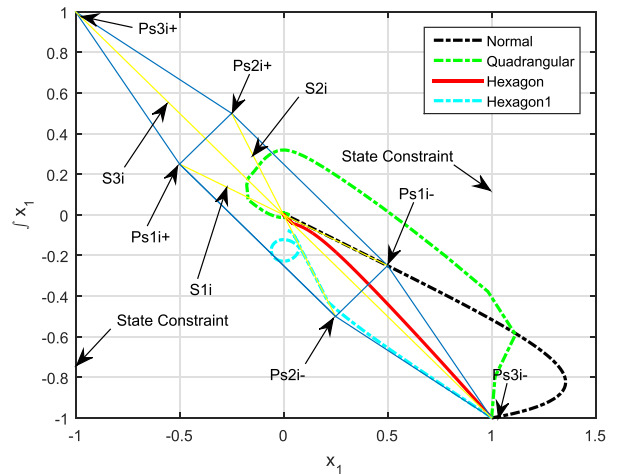| Params Options	ξ_{1i}	ξ_{2i}	ξ_{3i}	N_1	N_2
Normal	2	Null	Null	$10tanh(S_1)$	$10tanh(S_2)$
Quad	2	0.5	Null	0.6	0.3
Hexagon	2	0.5	1	0.6	0.3
Hexagon1	2	0.5	1	0.01	0.01

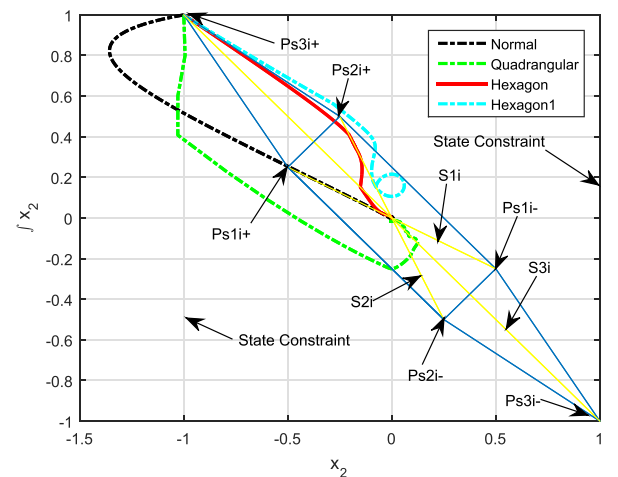**FIGURE 7.** Point (x_1, $\int x_1$) trajectory.

FIGURE 8. Point (x_2, $\int x_2$) trajectory.

As shown in figures 7-12, the state control effect has indeed been improved by UAS-SMC using four auxiliary surfaces (Quadrangular). However the trajectory of boundary
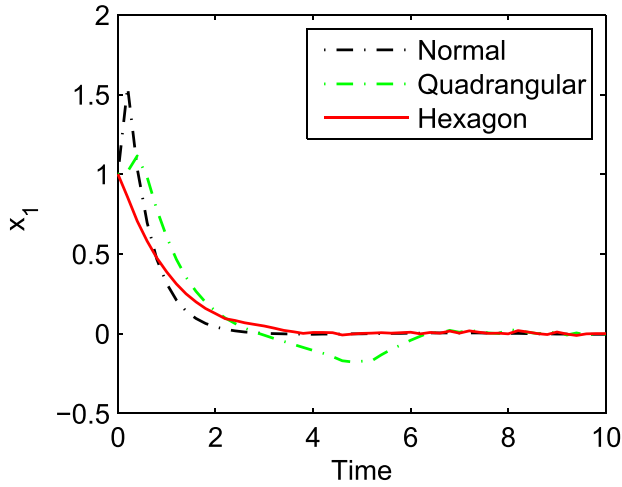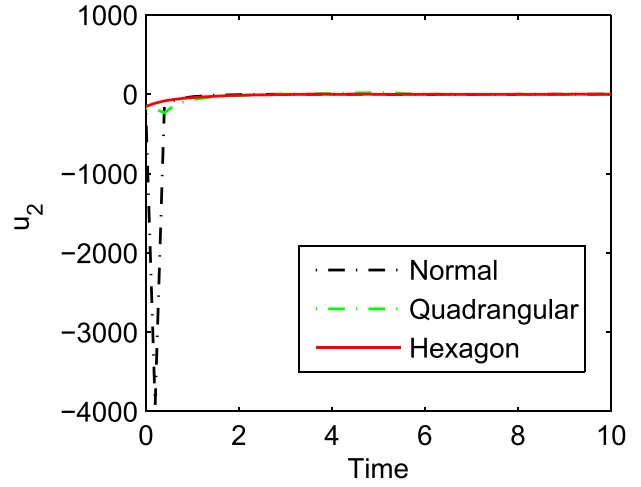
FIGURE 9. State x_1 trajectory.
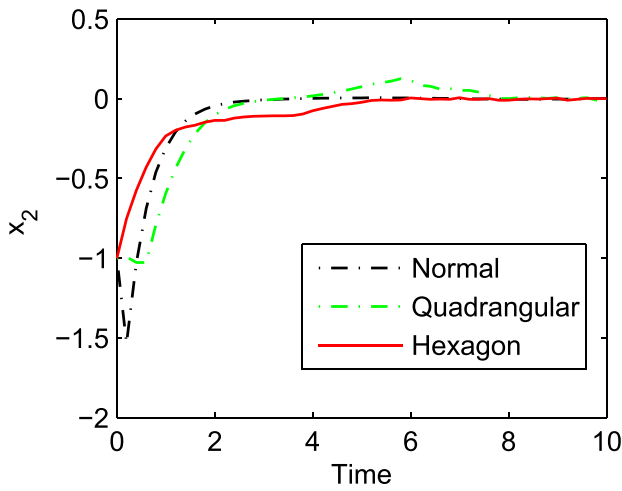

FIGURE 10. State x_2 trajectory.

FIGURE 11. Control input u_1.

FIGURE 12. Control input u_2.

FIGURE 13. Auxiliary surface H_1.

surfaces (Hexagon) can perform well and the hexagon enclosed by six auxiliary surfaces in blue color is a PIS. This means that once the system state enters into this hexagon, it will not leave this area even if the bounded disturbance has a magnitude of 0.2. This is a very important property in engineering applications on systems with constrained states.

It can be observed from Figure 13 and Figure 14, H_i changes according to the subspaces divided by S_{1i}, S_{2i}, S_{3i}. In different subspaces, H_i changes when the system state changes, and finally approaches zero. The focus of this paper is to show the benefits of the extension of the positive invariant set. We did not discuss in the Scenario A that the input dimension m is not equal to the state dimension n because we want to show that each state is restricted. The example in Scenario A was originally an inverted pendulum model, and we added a control input to better show that there is a good constraint on each state. In fact, for the typical 1 input and 2 outputs system model of inverted pendulum, the auxiliary surface sliding mode control method still has the ability of state constraint as shown in [28]. Scenario B shows that two states are controlled and constrained with only one control input by using AS-SMC method.
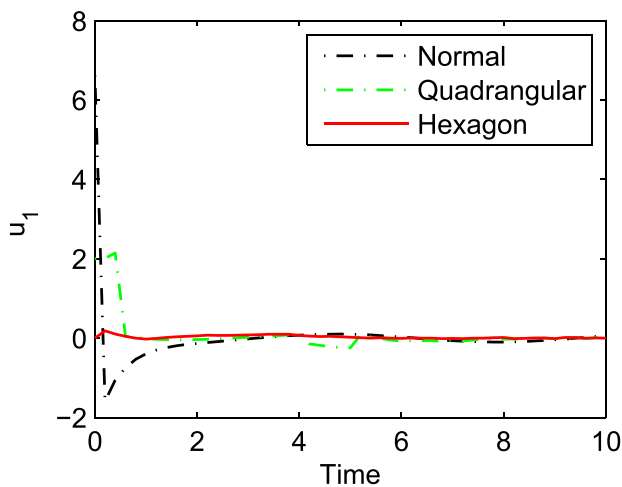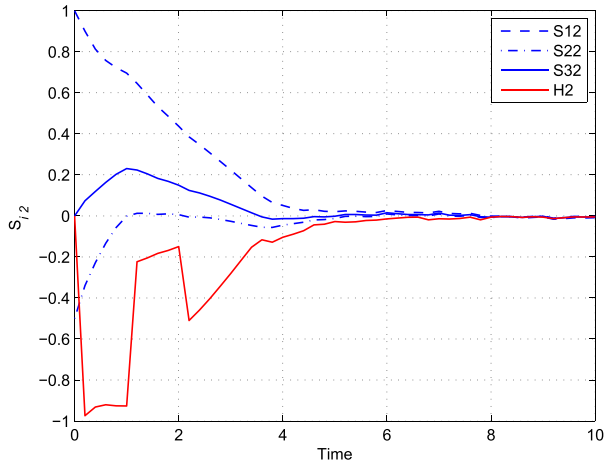
SMC (Normal) and UAS-SMC using four auxiliary surfaces show that they are still unable to meet the requirements of state constraints ϖ. AS-SMC using six auxiliary

FIGURE 14. Auxiliary surface H_2.

B. SCENARIO B: AUXILIARY SURFACES SLIDING MODE CONTROL FOR UNMANNED HELICOPTER ON A HARDWARE-IN-THE-LOOP PLATFORM

In real flight of unmanned helicopters, there are always reasons such that the attitude information cannot be fed back to the flight controller timely. For example: when the inertial navigation system fails temporarily, the flight controller is switched between master and slave. External influences, such as wind disturbance, will inevitably produce a significant change in attitude. When everything is back to normal, the unmanned helicopter may be in an extreme flight condition such as to be overturn. In this case, the flight controller needs to give a control input, so that the unmanned helicopter does not exceed the maximum constraint range to avoid tipping.

In Scenario B, AS-SMC using PIS is tested for an unmanned helicopter on a hardware-in-the-loop (HIL) platform to simulate the above situation. The complete nonlinear equation for unmanned helicopters is based on the formulas (1)-(5) in [3]. Since the constraint of the roll angle is symmetry, in order to facilitate the comparison of the Symmetric Barrier Lyapunov Functions (SBLF) method with our method [19], we use the model of roll channel for detailed explanation. The tracking error model equations of roll channel are given as follows:

$$\begin{cases} \dot{\phi}_e = p_e + \eta \\ \dot{p}_e = f(X) + g(X)M_x(\delta_{lat}) \end{cases} \quad (30)$$

where $X = [\phi_e, p_e]^T$ is the system state, ϕ_e is the roll angle error, p_e are the roll angle rate error, $\eta = \sin\phi \cdot \tan\theta \cdot q + \cos\phi \cdot \tan\theta \cdot r$ is treated as the disturbance, $f(X) = -(I_z - I_y)/I_x \cdot q \cdot r$, $g(X) = 1/I_x$, $M_x(\delta_{lat}) = K\_Y_{mr} \cdot T_{mr1} \cdot sin(\delta_{lat}) \cdot D_z + L_{df}$ is the rolling moment, K_Y_{mr} is the thrust coefficient, T_{mr} is the thrust of the main rotor, D_z represents the distance between the hub and the center of the gravity, L_{df} is the ducted fuselage moments produced by aerodynamic forces, δ_{lat} is the control input representing the lateral cyclic commands.

Before the start of the HIL simulation, we set the initial values of roll angle $\phi_e(t_0) = -35°(0.6109rad)$, and the roll angular rate $p_e(t_0) = 70°/s(1.2217rad/s)$. The roll angle constraints are $\varpi = \{\phi_e \mid -35° \leq \phi_e \leq 35°\}$, and the roll angular rate constraints are $\gamma = \{p_e \mid -70°/s \leq p_e \leq 70°/s\}$. In order to meet the actual angular rate constraint of the HIL platform, the roll angular rate should be within the constraints too.

The sliding surface $\acute{S}$ and the approaching law $\acute{N}$ of the normal integral SMC are

$$\acute{S} = I_1 \cdot p_e + \xi_1 \cdot \int p_e, \quad \acute{N} = -N_1 \cdot tanh(\acute{S})$$

where $I_1 = 1$, $\xi_1 = 4$, $N_1 = 10$. Neglecting the effects of disturbance η in the first formula of (30), $\phi_e = \int p_e$ can be obtained. Thus the sliding surface can be written as $\acute{S} = I_1 \cdot p_e + \xi_1 \cdot \phi_e$.

Following the steps in Section 3, the AS-SMC controller design process is presented as follow:

First, the switching surfaces are chosen as $S_1(X) = p_e + 4 \cdot \int p_e = p_e + 4 \cdot \phi_e$, $S_2(X) = p_e + 1 \cdot \int p_e = p_e + 1 \cdot \phi_e$, $S_3(X) = p_e + 2 \cdot \int p_e = p_e + 2 \cdot \phi_e$.

Second, for roll angle error ϕ_e and the roll angular rate p_e, we choose points as $P_{S1i+} = (-1.1335, 0.2835)$, $P_{S1i-} = (1.1335, -0.2835)$, $P_{S2i+} = (-0.5665, 0.5665)$, $P_{S2i-} = (0.5665, -0.5665)$, $P_{S3i+} = (-1.7, 0.85)$, $P_{S3i-} = (1.7, -0.85)$. Thus the auxiliary surface $H_1 = \omega_{11_1}p_e + \omega_{11_2}\int p_e + M_1 = \omega_{11_1}p_e + \omega_{11_2}\phi_e + M_1$ for state p_e and ϕ_e can be obtained, where

$$\omega_{11_1} = \begin{cases} 1, & No.0_i \\ 1, & No.1_i \\ -1, & No.2_i \\ -1, & No.3_i \\ -1, & No.4_i \\ 1, & No.5_i \end{cases} \omega_{11_2} = \begin{cases} 2, & No.0_i \\ 4, & No.1_i \\ -1, & No.2_i \\ -2, & No.3_i \\ -4, & No.4_i \\ 1, & No.5_i \end{cases}$$

$$M_1 = \begin{cases} 0.5665, & No.0_i \\ 1.7, & No.1_i \\ 0.85, & No.2_i \\ 0.5665, & No.3_i \\ 1.7, & No.4_i \\ 0.85, & No.5_i \end{cases}$$

Finally, the AS-SMC controller is $u = [\omega_{11_1}g(X)]^{-1}[-\omega_{11_1}f(X) - \omega_{11_2}p_e + N]$, where $N = 0.05$.

The boundary layer SMC (shown as 'Normal' in figures), the Symmetric Barrier Lyapunov Functions (shown as 'SBLF' in figures) and AS-SMC using six auxiliary surfaces (shown as 'AS-SMC' in figures) are compared in Scenario B. Following the above steps, we get HIL simulation results shown in Figure 15 to Figure 18.

As can be seen from Fig.15, the normal method does satisfy the roll angle constraint, but the roll angular rate constraint is not satisfied. By setting the control gains
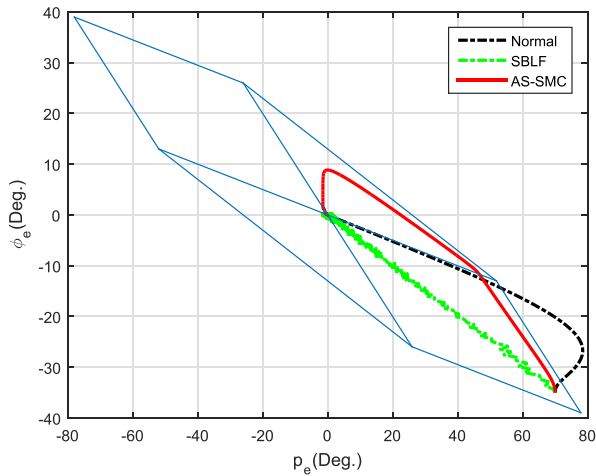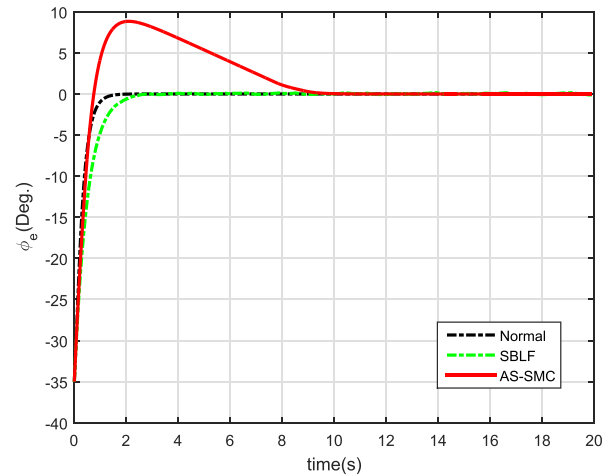
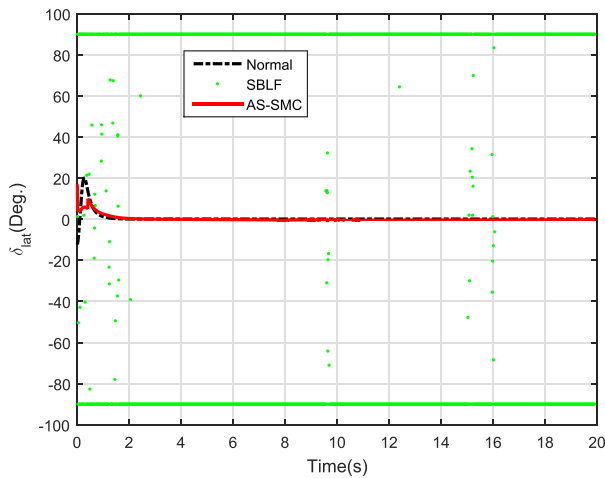**FIGURE 15. Point (p_e, ϕ_e) trajectory.**
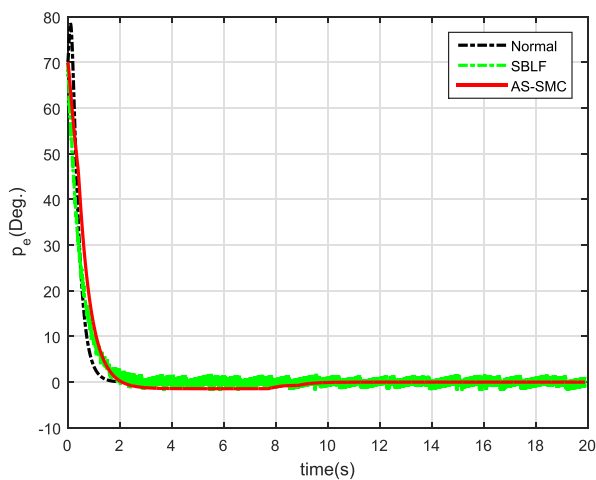

FIGURE 16. Control output $\delta_l at$.

FIGURE 17. Roll angle error p_e.

$k_1 = k_2 = 2$, $k_{b1} = 35$, the SBLF method appears to satisfy the constraints of the roll angle. However, the output of the SBLF controller switches back and forth between ±90°. This is because the SBLF method requires a very large rolling

FIGURE 18. Roll angular rate error ϕ_e.

moment to achieve attitude control. When the $sin(\delta_{lat})$ is reversely solved by the rolling moment M_x, the control output is switched between ±90° due to $sin(\delta_{lat})$ exceeding ± 1. Moreover, the roll angular rate is not well controlled due to the control output chattering. As can be seen from Fig. 17, p_e always has a chattering phenomenon during the convergence process, which further causes the chattering of ϕ_e.

The constraints of the roll angle and the roll angular rate are simultaneously satisfied by the AS-SMC method. At the same time, the output of the AS-SMC controller is also smooth enough. The HIL simulation tests indicate good results for keeping balance of the UH even in the extreme initial values under the control of AS-SMC by using PIS. The extension of positive invariant set is not a simple extension of four auxiliary surfaces, but the best choice to achieve satisfied control effect for some of the extreme initial conditions and constrained system states. The algorithm is an improvement over previous algorithms.

By comparing these three control methods, it is not difficult to find that when the PIS-SMC strategy is adopted, the system states converge to the origin more slowly than the other two control strategy. This is because AS-SMC's control input is much smaller than that of Normal's control input. Future work will be focused on how to speed up the state convergence rate of the auxiliary surfaces sliding mode control under the premise of satisfying the constraint conditions. This may require a trade-off between the AS-SMC and Normal SMC for the size of the control input.

VI. CONCLUSION

This paper presents a new control strategy named positive invariant set by using auxiliary surfaces sliding mode. Compared to the previous auxiliary surfaces sliding mode controller, this strategy adds one sliding surface and two auxiliary surfaces. Although this design strategy increases the complexity of the controller design, the area of the positive invariant set is expanded. In this way, the sliding mode phase starts from the boundary of the state constraints, so that

the system is robust with respect to uncertainties. It has an important theoretical significance and an application value, and the control strategy is in line with the actual needs of engineering.

REFERENCES

[1] O. Barambones, P. Alkorta, and J. M. G. de Durana, "A real-time estimation and control scheme for induction motors based on sliding mode theory," *J. Franklin Inst.*, vol. 351, no. 8, pp. 4251–4270, 2014.

[2] F. Blanchini, "Survey paper: Set invariance in control," *Automatica*, vol. 35, no. 11, pp. 1747–1767, 1999.

[3] Z. Chen, D. Wang, Z. Zhen, B. Wang, and J. Fu, "Take-off and landing control for a coaxial ducted fan unmanned helicopter," *Aircr. Eng. Aerosp. Technol.*, vol. 89, no. 6, pp. 764–776, 2017.

[4] C. Zhi, W. Daobo, Z. Ziyang, and W. Biao, "Modeling and sliding mode control with boundary layer for unmanned coaxial rotor ducted fan helicopter," *Trans. Nanjing Univ. Aeronaut. Astronaut.*, vol. 33, no. 2, pp. 199–207, 2016.

[5] J. Davila and A. Poznyak, "Sliding mode parameter adjustment for perturbed linear systems with actuators via invariant ellipsoid method," *Int. J. Robust Nonlinear Control*, vol. 21, no. 5, pp. 473–487, 2011.

[6] R. A. DeCarlo, S. H. Zak, and G. P. Matthews, "Variable structure control of nonlinear multivariable systems: A tutorial," *Proc. IEEE*, vol. 76, no. 3, pp. 212–232, Mar. 1988.

[7] J. Fu, Q.-X. Wu, and Z.-H. Mao, "Chattering-free SMC with unidirectional auxiliary surfaces for nonlinear system with state constraints," *Int. J. Innov. Comput., Inf. Control*, vol. 9, no. 12, pp. 4793–4809, 2013.

[8] W. B. Gao, *Theory and Design Method of Variable Structure Control*. Beijing, China: Science Press, 1996.

[9] C. Han, L. Yang, and J. Zhang, "Adaptive nonsingular fast terminal sliding mode control for aircraft with center of gravity variations," *Proc. Inst. Mech. Eng. G, J. Aerosp. Eng.*, vol. 229, no. 1, pp. 4–9, 2015.

[10] S. Han, B. Cho, S.-H. Son, K.-B. Park, and T. Tsuji, "Sliding mode controller with nonlinear sliding surface for a second order system with input saturation," in *Proc. Annu. Conf. IEEE Ind. Electron. Soc. (IECON)*, vol. 3, Nov. 2004, pp. 2159–2162.

[11] S. Laghrouche, F. Plestan, and A. Glumineau, "Higher order sliding mode control based on integral sliding mode," *Automatica*, vol. 43, no. 3, pp. 531–537, 2007.

[12] Y. V. Orlov, *Discontinuous Systems: Lyapunov Analysis and Robust Synthesis Under Uncertainty Conditions*. Berlin, Germany: Springer, 2008.

[13] O. Pastravanu and M.-H. Matcovschi, "Linear time-variant systems: Lyapunov functions and invariant sets defined by Hölder norms," *J. Franklin Inst.*, vol. 347, no. 3, pp. 627–640, 2010.

[14] A. Polyakov and A. Poznyak, "Invariant ellipsoid method for minimization of unmatched disturbances effects in sliding mode control," *Automatica*, vol. 47, no. 7, pp. 1450–1454, 2011.

[15] A. Rauh, J. Kersten, and H. Aschemann, "Interval-based implementation of robust variable-structure and backstepping controllers of single-input single-output systems," *IFAC-PapersOnLine*, vol. 50, no. 1, pp. 6283–6288, 2017.

[16] A. Rauh, L. Senkel, and H. Aschemann, "Interval methods for variable-structure control of dynamic systems with state constraints," in *Proc. 3rd Conf. Control Fault-Tolerant Syst. (SysTol)*, Sep. 2016, pp. 466–471.

[17] H. Richter, B. O'Dell, and E. A. Misawa, "Robust positively invariant cylinders in constrained variable structure control," *IEEE Trans. Autom. Control*, vol. 52, no. 11, pp. 2058–2069, Nov. 2007.

[18] A. Sabanovic, M. Elitas, and K. Ohnishi, "Sliding modes in constrained systems control," *IEEE Trans. Ind. Electron.*, vol. 55, no. 9, pp. 3332–3339, Sep. 2008.

[19] K. P. Tee, S. S. Ge, and E. H. Tay, "Barrier Lyapunov functions for the control of output-constrained nonlinear systems," *Automatica*, vol. 45, no. 4, pp. 918–927, Apr. 2009.

[20] V. Utkin, J. Guldner, and J. Shi, *Sliding Mode Control in Electro-Mechanical Systems*, 2nd ed. Boca Raton, FL, USA: Taylor & Francis, 2009.

[21] M. Wu, G. Yan, Z. Lin, and M. Liu, "Characterization of backward reachable set and positive invariant set in polytopes," in *Proc. Amer. Control Conf.*, Jun. 2009, pp. 4351–4356.

[22] L. Zhao and Y. Jia, "Distributed adaptive containment control for second-order multi-agent systems via NTSM," *J. Franklin Inst.*, vol. 352, no. 11, pp. 5327–5341, 2015.

[23] L. Zhao and Y. Jia, "Finite-time attitude tracking control for a rigid spacecraft using time-varying terminal sliding mode techniques," *Int. J. Control*, vol. 88, no. 6, pp. 1150–1162, Jan. 2015.

[24] J. Zhang, L. Yang, and G. Shen, "New hybrid adaptive control approach for aircraft with centre of gravity variation," *IET Control Theory Appl.*, vol. 6, no. 14, pp. 2179–2187, Sep. 2012.

[25] B. Zhou, G.-R. Duan, and Z. Lin, "Approximation and monotonicity of the maximal invariant ellipsoid for discrete-time systems by bounded controls," *IEEE Trans. Autom. Control*, vol. 55, no. 2, pp. 440–446, Feb. 2010.

[26] J. Fu, L. Wang, M. Chen, and S. Chang, "Robust adaptive attitude control for airbreathing hypersonic vehicle with attitude constraints and propulsive disturbance," *Math. Problems Eng.*, vol. 2015, Nov. 2015, Art. no. 293480.

[27] J. Fu, L. Wang, and M. Chen, "Invariant set based sliding mode control for near-space vehicles with attitude constraints," *Proc. Inst. Mech. Eng., G, J. Aerosp. Eng.*, vol. 230, no. 5, pp. 793–804, 2016.

[28] J. Fu, Q. X. Wu, C. S. Jiang, and Y. F. Wang, "Robust sliding mode positively invariant set for nonlinear continuous system," *Acta Automatica Sinica*, vol. 37, no. 11, pp. 1395–1401, 2011.

[29] S. Xiao, S. Liu, F. Jiang, M. Song, and S. Cheng, "Nonlinear dynamic response of reciprocating compressor system with rub-impact fault caused by subsidence," *J. Vib. Control*, vol. 25, no. 11, pp. 1737–1751, 2019.

[30] L. Zhang, Z. Yi, S. L. Zhang, and P. A. Heng, "Activity invariant sets and exponentially stable attractors of linear threshold discrete-time recurrent neural networks," *IEEE Trans. Autom. Control*, vol. 54, no. 6, pp. 1341–1347, Jun. 2009.
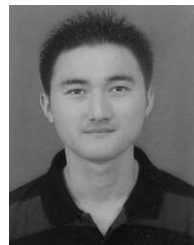
ZHI CHEN received the Ph.D. degree from the College of Automation Engineering, Nanjing University of Aeronautics and Astronautics, in 2017.

From 2016 to 2017, he was a Visiting Scholar with the National University of Singapore. Since 2017, he has been a Postdoctoral Research Fellow with the Mechatronic Engineering and Automation Department, Shanghai University. His research interests include sliding mode variable structure control and the design and control of unmanned aerial vehicles, especially the modeling and design of unmanned helicopters.

Dr. Chen served as the Principal Investigator with the China Postdoctoral Science Foundation.
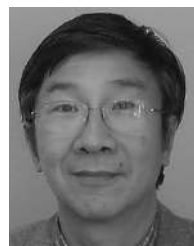
XIAOWEI TU received the bachelor's degree in computer science from Shanghai Jiao Tong University, China, and the master's and Ph.D. degrees in computer vision and image processing from the University of Technology of Compiègne, France, in 1982 and 1987, respectively.

From 1988 to 1997, he was a Professor and then a Research Scientist in real-time vision system design, mobile robots, and pattern-recognition fields with the French National Research Center, France. From 1998 to 2006, he was with the Industrial Research Center of Quebec, Canada, where he was a Research and Development Scientist and Engineer involved in the field of robotic vision and industrial inspection projects. From 2006 to 2011, he was a Senior Researcher with the Aerospace Manufacturing Technology Centre, National Research Council of Canada, where he was involved in the projects of visual serving for robots, surface inspection, and integration of automation systems in aerospace industries. Since 2011, he has been a Faculty Member with the Mechatronics and Automation Institute, Shanghai University, involved in the research and development projects on sensors and control systems for autonomous vehicles.

LI XING received the Ph.D. degree from the College of Automation Engineering, Nanjing University of Aeronautics and Astronautics, in 2018.

Since 2018, she has been a Postdoctoral Research Fellow with the Mechatronic Engineering and Automation Department, Shanghai University. Her research interest includes the data fusion algorithm of navigation sensors on the unmanned aerial vehicles, in indoor and outdoor environment.

JIAN FU received the Ph.D. degree from the College of Automation Engineering, Nanjing University of Aeronautics and Astronautics, in 2013.

From 2009 to 2010, he was a Visiting Student with Loughborough University, U.K. Since 2014, he has been the Principal Investigator with the China Postdoctoral Science Foundation. From 2014 to 2018, he has been a Lecturer with the School of Energy and Power Engineering, Nanjing University of Science and Technology. Since 2018, he has been an Associate Professor of the Nanjing University of Science and Technology. His research interests include the control design of unmanned aerial vehicle and control theory, especially the sliding mode control theory.

ROGELIO LOZANO received the B.S. degree in electronic engineering from the National Polytechnic Institute of Mexico, in 1975, the M.S. degree in electrical engineering from the Centro de Investigación y de Estudios Avanzados (CINVESTAV), Mexico, in 1977, and the Ph.D. degree in automatic control from Laboratoire d'Automatique de Grenoble, France, in 1981.

From 1985 to 1987, he was the Head of the Section of Automatic Control. He was the Head of the Heudiasyc Laboratory, from 1995 to 2007. Since 1990, he has been a Research Director with the Centre National de la Recherche Scientifique (CNRS), University of Technology of Compiègne, France. He is the Head of the Joint Mexican-French UMI 3175 CNRS. He has been the advisor or co-advisor of more than 35 Ph.D. theses and published more than 130 international journal papers and 10 books. His research interests include UAVs, mini-submarines, exo-squelettons, and automatic control.

Dr. Rogelio has coordinated or participated in numerous French projects dealing with UAVs. He has recently organized two international workshops on UAVs (IFAC RED UAS 2013 and IEEE RAS RED UAS 2015). He has been participating the annual International Conference on Unmanned Aerial Systems (ICUAS), since 2010. He was an Associate Editor of *Automatica*, from 1987 to 2000. He is an Associate Editor in the *International Journal of Adaptive Control and Signal Processing* and the *Journal of Intelligent and Robotics Systems*.

• • •